Cell Reports
Methods

Article

Microparticle immunocapture assay for quantitation of protein multimer amount and size

Graphical abstract

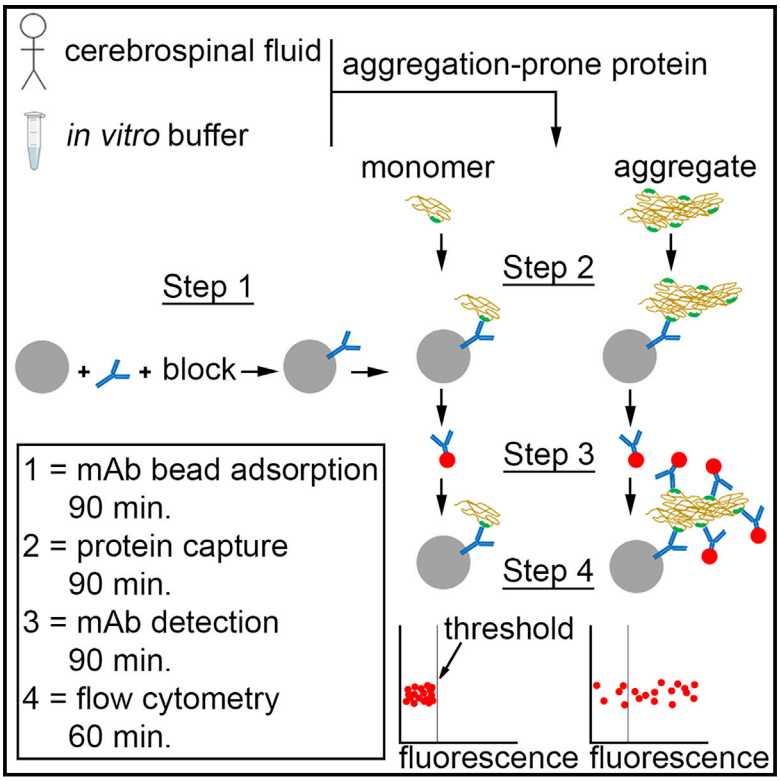

Authors

Michael F. Gutknecht, Hiroaki Kaku, Thomas L. Rothstein

Correspondence

tom.rothstein@med.wmich.edu

In brief

Protein aggregate formation is associated with several human pathologies and is a complicating factor in the development of pharmaceutical agents. Gutknecht et al. present a microparticle, antibody-mediated capture platform that permits the specific detection and quantitation of protein aggregate amount and size, while ignoring monomers, in a streamlined workflow.

Highlights

- A simple, straightforward, and quick assay to characterize protein aggregates
- Simultaneous assessment of protein aggregate size and amount
- Adaptable to any protein for which suitable antibody reagents exist
- Demonstrates application to CSF samples

Gutknecht et al., 2022, Cell Reports Methods 2, 100214
May 23, 2022
https://doi.org/10.1016/j.crmeth.2022.100214

CellPress

Cell Reports Methods

CellPress
OPEN ACCESS

Article

Microparticle immunocapture assay for quantitation of protein multimer amount and size

Michael F. Gutknecht,[1] Hiroaki Kaku,[1] and Thomas L. Rothstein[1,2,*]
[1]Department of Investigative Medicine and Center for Immunobiology, Western Michigan University Homer Stryker M.D. School of Medicine, Kalamazoo, MI, USA
[2]Lead contact
*Correspondence: tom.rothstein@med.wmich.edu
https://doi.org/10.1016/j.crmeth.2022.100214

MOTIVATION Protein aggregates, also known as protein multimers or dysfunctional or disordered protein deposits, are known to be associated pathogenically with neurodegenerative and other diseases. Accurate measurement of protein aggregates during *in vitro* work and with clinical samples is imperative. However, currently available methods are limited in providing a measure of protein aggregate size. We present a microparticle bead-based immunocapture assay that provides, at the same time, measurement of protein aggregate amount and size. The assay is simple, specific, quantitative, and quick, providing results within a single experimental day.

SUMMARY

Cellular stress and toxicity are often associated with the formation of protein multimers, or aggregates. Numerous degenerative disorders, including Alzheimer's, Parkinson's, and Huntington's disease, prion-propagated disease, amyotrophic lateral sclerosis, cardiac amyloidosis, and diabetes, are characterized by aggregated protein deposits. Current methods are limited in the ability to assess multimer size along with multimer quantitation and to incorporate one or more ancillary traits, including target specificity, operative simplicity, and process speed. Here, we report development of a microparticle immunocapture assay that combines the advantages inherent to a monoclonal antibody:protein interaction with highly quantitative flow cytometry analysis. Using established reagents to build our platform, and aggregation-prone amyloid beta 1-42 peptide (Aβ42) and alpha-synuclein to demonstrate proof of principle, our results indicate that this assay is a highly adaptable method to measure multimer size and quantity at the same time in a technically streamlined workflow applicable to laboratory and clinical samples.

INTRODUCTION

Protein aggregation is the formation of multimer assemblies from disordered mutant or damaged protein monomers. In such situations, established control mechanisms fail to sufficiently induce proper protein refolding or to adequately remove unrecoverable proteins for degradation via proteosome and autophagy mechanisms (Mogk et al., 2018; Tanaka and Matsuda, 2014). In addition to direct toxicity, protein aggregates are thought to be harmful through loss of function related to deficient physiology of proteins now aggregated and nonfunctional, and/or to exhaustion of remediating mechanisms. The connection between aggregate formation and disease is widespread, encompassing neuro-pathologies such as Alzheimer's disease (amyloid, tau), Parkinson's disease (alpha-synuclein [αS]), Huntington's disease (huntingtin), prion-propagated disease (PrP), and amyotrophic lateral sclerosis (TDP-43, SOD1, FUS, and more), as well as disease in other tissues, such as the heart (cardiac amyloidosis) and pancreas (type II diabetes, islet cell IAPP). This is most strikingly illustrated in brain sections from Alzheimer's disease patients, where immunohistochemical detection and visualization of beta-amyloid and tau protein deposits scattered in large abundance are routinely observed and correlate with disease severity (Aguzzi and O'Connor, 2010; Haass and Selkoe, 2007).

Although the means by which protein aggregates damage cells remain uncertain, the need for robust and accurate quantitative methods to distinguish between protein monomers and aggregated multimers, and to evaluate the amount and size of protein aggregates, is clear yet has not been fully addressed (Cox et al., 2020). This applies to basic research, where the proteostatic activity of chemical compounds and biological molecules is determined, as well as clinical diagnostics, where plasma neuro-protein aggregate detection is rapidly becoming more accepted as an indicator of neurodegenerative disease (Lindquist and Kelly, 2011; Palmqvist et al., 2020; Shahnawaz et al., 2017; Tokuda et al., 2010). In addition, the need to

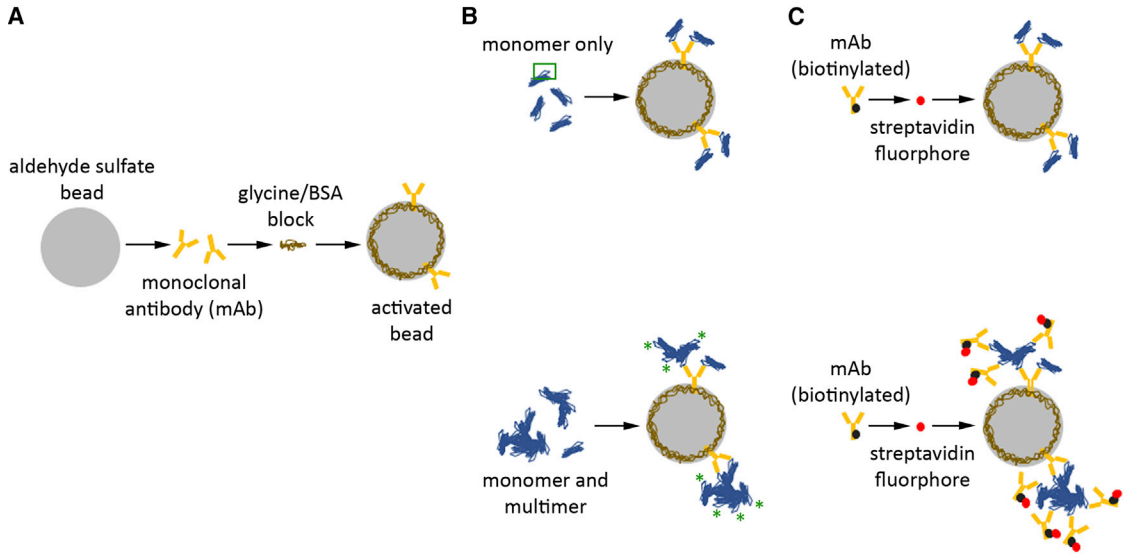

Figure 1. Assay schematic

(A) Monoclonal antibodies (mAb) specific for an aggregation-prone protein are adsorbed onto super active aldehyde sulfate microbeads. The remaining active sites on beads are blocked with irrelevant protein such as bovine serum albumin (BSA).

(B) The bead-mAb combination is incubated with the target protein. Illustrated are examples for solutions containing non-aggregated protein monomer only (top row) or monomers and multimers (bottom row). mAb-target protein binding occurs at a specific site (green box). All antibody binding sites on bound monomers are saturated, whereas unoccupied binding sites exist on bound multimers (green asterisks).

(C) The bead-mAb-target protein complex is incubated sequentially with the identical monoclonal antibody (biotinylated) and streptavidin fluorophore, followed by fluorescence detection and quantitation.

accurately identify and quantitate aggregated contaminants in pharmaceutical sample preparations is essential in the development and production of safe bioactive compounds. Several methods and tools have been adapted to evaluate protein aggregation, including electron microscopy, light scattering, electrophoretic migration, and enzyme-linked immunosorbent assay (ELISA), among others, with each having its own set of advantages and limitations (Bagriantsev et al., 2006; Chaudhuri et al., 2014; den Engelsman et al., 2011; El-Agnaf et al., 2006; Mahler et al., 2009). However, none combine quantification of degree of aggregation (e.g., ELISA) and size of aggregates (e.g., electrophoresis). In addition, none combine these characteristics with target specificity, ease of use, speed of results, and availability of needed instrumentation.

In this report, we present a microparticle immunocapture fluorescence assay to quantify protein aggregation by flow cytometry. We designed this assay to be specific for the protein of interest, to distinguish protein monomer from multimer, to determine both aggregate amount and size, to be performed with standard laboratory equipment, and to be neither time nor resource intensive. We utilized super active aldehyde sulfate microbeads for the bead platform and tested the aggregation-prone protein amyloid beta 1-42 (Aβ42) as proof-of-principle. Both reagents have been documented extensively in the literature, and Aβ42 aggregation has wide-ranging interest in neurological disease research (Cheng et al., 2018; Mendt et al., 2018; O'Brien and Wong, 2011; Suárez et al., 2017; Théry et al., 2006; Wahlgren et al., 2012; Wang et al., 2017). We then applied bead assay analysis to a second aggregation-prone and clinically relevant protein, αS, demonstrating again the assay characteristics of target specificity and protein multimer-specific detection, as well as aggregate detection in human cerebrospinal fluid (CSF). Our results demonstrate successful development of a specific, target protein-adaptable, simple, and comparatively rapid assay for protein multimer detection and quantitation, as well as characterization of multimer size. We envision many potential applications to the study of protein aggregation in basic, clinical, and pharmaceutical settings as this method only requires materials, equipment, and scientific expertise that are present in many basic research and clinical research laboratories.

RESULTS

Assay overview

The fluorescent microparticle immunocapture assay for protein aggregation described herein involves three steps (Figure 1). Super active aldehyde sulfate beads are utilized as a microparticle platform upon which an epitope-specific, monoclonal capture antibody is bound by covalent interaction (Figure 1A). After blocking with irrelevant protein, the loaded beads are incubated with a test solution containing the protein of interest, leading to antibody-protein interaction (Figure 1B, binding epitope, green box) and subsequent protein capture and presentation on the bead surface. No unoccupied binding sites should exist on captured monomeric proteins due to antibody binding the single epitope, whereas unoccupied binding sites, or detection sites, will exist on captured protein multimers (Figure 1B, green asterisks). A subsequent two-step incubation with the identical monoclonal antibody (mAb) (biotinylated) and then streptavidin (SA)

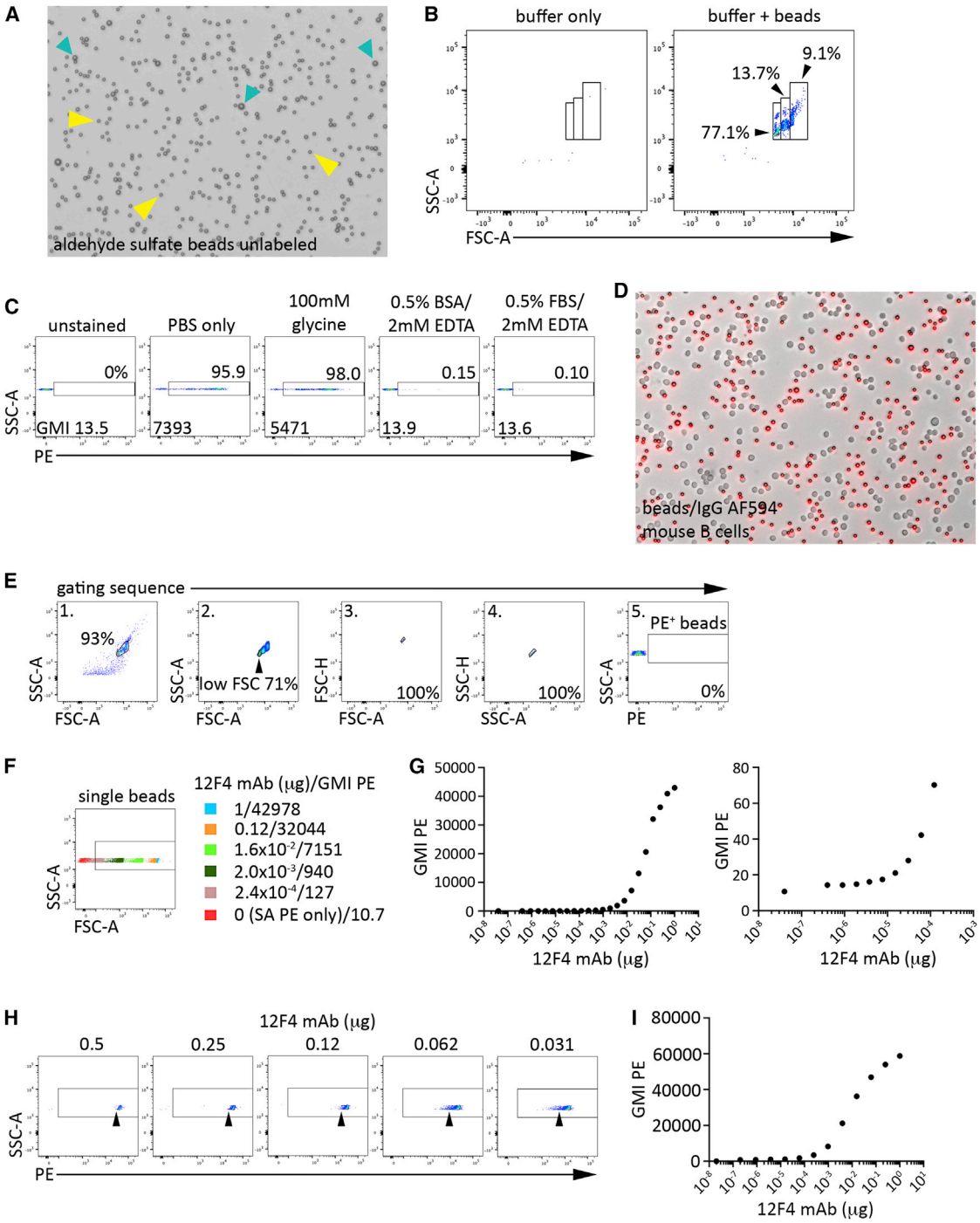

Figure 2. Characterization and antibody binding properties of aldehyde sulfate beads

(A) Microscopic bright-field image of unlabeled beads. Yellow arrowheads denote the most prevalent, comparatively smaller diameter beads. Turquoise arrowheads denote the less numerous larger diameter beads. 20× magnification.

(B) Flow cytometry dot plot of buffer only (left) or buffer + beads (right). Three gated populations distinguished by the physical parameters of size (FSC-A) and complexity/granularity (SSC-A) are shown. The majority of beads (77.1%) fall within the low FSC-A gate.

(C) Beads were first incubated with the indicated PBS-based blocking buffer preparation for 60 min, then with IgG phycoerythrin (PE) (0.0025 μg/μL) for 30 min, and subsequently analyzed by flow cytometry. Dot plots display the percentage of PE^+ beads and geometric mean intensity (GMI) PE of the low FSC-A bead population.

(D) Beads labeled with IgG AF594 were blocked with BSA, mixed at equal number with sorted murine B cells, and imaged. 20× magnification.

(legend continued on next page)

fluorophore allows detection of only protein multimers, while bound monomers go undetected (Figure 1C). More unoccupied detection sites in larger multimers result in more antibody/SA fluorophore binding, and hence greater fluorescence. The fluorescence signal of individual beads is then quantitated by flow cytometer acquisition and analysis.

Aldehyde sulfate bead protein-binding characteristics and flow cytometry acquisition

Although aldehyde sulfate bead use in research is well documented, we validated the physical nature of the beads and the bead properties required for assay function, including capture antibody adsorption onto beads and detection by flow cytometry (Mendt et al., 2018; Suárez et al., 2017; Théry et al., 2006; Wahlgren et al., 2012). Aldehyde sulfate bead stock imaged by bright-field microscopy displayed a population that was largely uniform in diameter (yellow arrows), with a small percentage of larger diameter beads (turquoise arrows) (Figure 2A). Bead populations could be visualized on a standard flow cytometry dot plot (see gated bead populations [right] versus buffer alone [left]) using the physical parameters of size (FSC-A, x axis) and complexity (SSC-A y axis) (Figure 2B). The relative proportion of bead populations observed by microscopy was congruent with flow cytometry, with the large majority of beads (77.1%) in the lower FSC population. Glycine, followed by incubation and washes in a blocking agent such as BSA, is reported in the literature as an effective block of non-specific protein adsorption to beads (Théry et al., 2006). To demonstrate this, we first incubated beads with buffers of predicted variable blocking efficiencies, followed by incubation with fluorescent antibody. Flow cytometry analysis and quantitation of the geometric mean intensity of PE (GMI PE) indicated that beads incubated in 100 mM glycine/PBS were blocked to some extent (GMI PE 5,471 versus 7,393 for PBS alone); however, addition of an irrelevant protein, such as BSA or FBS, provided a complete block of antibody binding (GMI PE 13.9 and 13.6 versus 13.5 for unstained beads) (Figure 2C). As an additional confirmatory step, we first labeled beads with fluorescent antibody, blocked in glycine/BSA, mixed beads with sorted B cells, and imaged the solution by bright-field microscopy. We observed fluorescently labeled beads of the expected size (4 μm bead versus 8–10 μm B cell) that were in solution unbound to the protein-rich surface of B cells (Figure 2D). Therefore, the blocking conditions of 100 mM glycine PBS followed by 0.5% BSA/2 mM EDTA PBS were utilized for the duration of our experiments.

We next determined 12F4 mAb-to-bead binding properties, with the goal to identify the amount of antibody that would provide near maximum binding potential to amyloid peptides in solution without reaching the coating saturation of the beads. Adsorption onto polystyrene substrates can result in protein layering at high concentrations, leading to unstable outer layers that can have an enhanced potential to dissociate from the substrate (Butler, 2000; Vogler, 2012). Titrated biotinylated-12F4 mAb (range of 4×10^{-7}–1 μg/50 μL) was incubated with 1 μL AS bead stock/50 μL (total incubation volume 100 μL), followed by block, wash, SA PE incubation, and flow cytometry acquisition and analysis. Application of a standard flow cytometry gating scheme to beads that received SA PE only (no 12F4 mAb) allowed the identification of single PE^+ beads (Figure 2E). Analysis of the 12F4 mAb titrated samples utilizing this scheme indicated that bead PE fluorescence increased with increasing 12F4 mAb concentration, up to 0.25 μg, whereupon the slope of the curve started to flatten (Figures 2F and 2G [left graph all titrated samples, right graph most dilute samples only]). A comparison of the dot plots from beads in the antibody range 0.031–0.5 μg showed a distinct sub-saturated fluorescence tail (black arrowhead) at levels below 0.25 μg, but not present at 0.5 μg (Figure 2H). We then conducted a 12F4 mAb titration using 10-fold less beads (0.1 μL bead stock/100 μL total volume) and observed a similar curve based on the 12F4 mAb:bead stock ratio (Figure 2I), thus indicating that bead adsorption at 0.4 μg 12F4 mAb/1.0 μL AS bead stock was sufficient to coat the beads to a high degree but remain below bead saturation.

Evaluation of 12F4 mAb binding to Aβ42, optimal analyte concentration, and assay sensitivity

The results to this point suggested that aldehyde sulfate beads constitute a suitable platform for immunocapture of a protein target. Although use of 12F4 mAb is reported in the literature, we confirmed that it could bind Aβ42 specifically under conditions dictated by the assay. We first incubated titrated monomeric Aβ42 directly with reactive beads to allow adsorption, followed by wash and then block. The samples were then incubated with an equivalent amount of biotinylated 12F4, followed by wash, SA PE incubation, wash, and flow cytometry analysis. As expected, increased amounts of Aβ42 resulted in higher bead fluorescence (Figure 3A), indicating that 12F4 mAb could bind Aβ42. A similar curve (based on Aβ42 (μg):bead stock ratio (μL); plateau ~0.1 μg:0.1 μL) was observed when

(E) Beads (1.0 μL bead stock/100 μL PBS) were incubated with titrated biotinylated anti-Aβ42 monoclonal antibody mAb (clone 12F4), blocked, incubated with an equivalent amount of streptavidin (SA)-phycoerythrin (PE), washed, and analyzed by flow cytometry. Dot plots display the gating scheme utilized to identify the low FSC-A singlet AS bead population for analysis. From left to right, the bead population was identified from all acquired events (1, 93%) using FSC-A and SSC-A. The low FSC-A population (2, black arrowhead; 71%) was subjected to FSC (3, 100%), and SSC (4, 100%) pulse width analysis to discriminate single beads from bead aggregates. The GMI PE of the resultant bead population (5) was determined for all samples (example shown for the SA PE only sample; gate indicates the PE^+ bead population).

(F) Overlay of representative dot plots showing the PE intensity and gated PE^+ beads for samples incubated with the indicated amount of 12F4 mAb. The color table to the right shows the GMI PE value for each of the 12F4 mAb titrations shown in the dot plot.

(G) Two graphs represent the bead GMI PE for all titrated 12F4 samples (left) and the most dilute 12F4 mAb samples only (right).

(H) Flow cytometry dot plots (bottom row) display the bead PE intensity for beads incubated with 0.5–0.031 μg 12F4 mAb, with beads that exhibited sub-maximal signal intensity highlighted by black arrowheads.

(I) Beads prepared at 0.1 μL bead stock/100 μL PBS were incubated with titrated biotinylated-12F4 mAb and analyzed by flow cytometry. The graph represents the bead GMI PE for all titrations. Due to the limitations of using a value of 0 on a log scale, the data points for the lowest amount of amyloid on all graphs represent 0 μg amyloid.

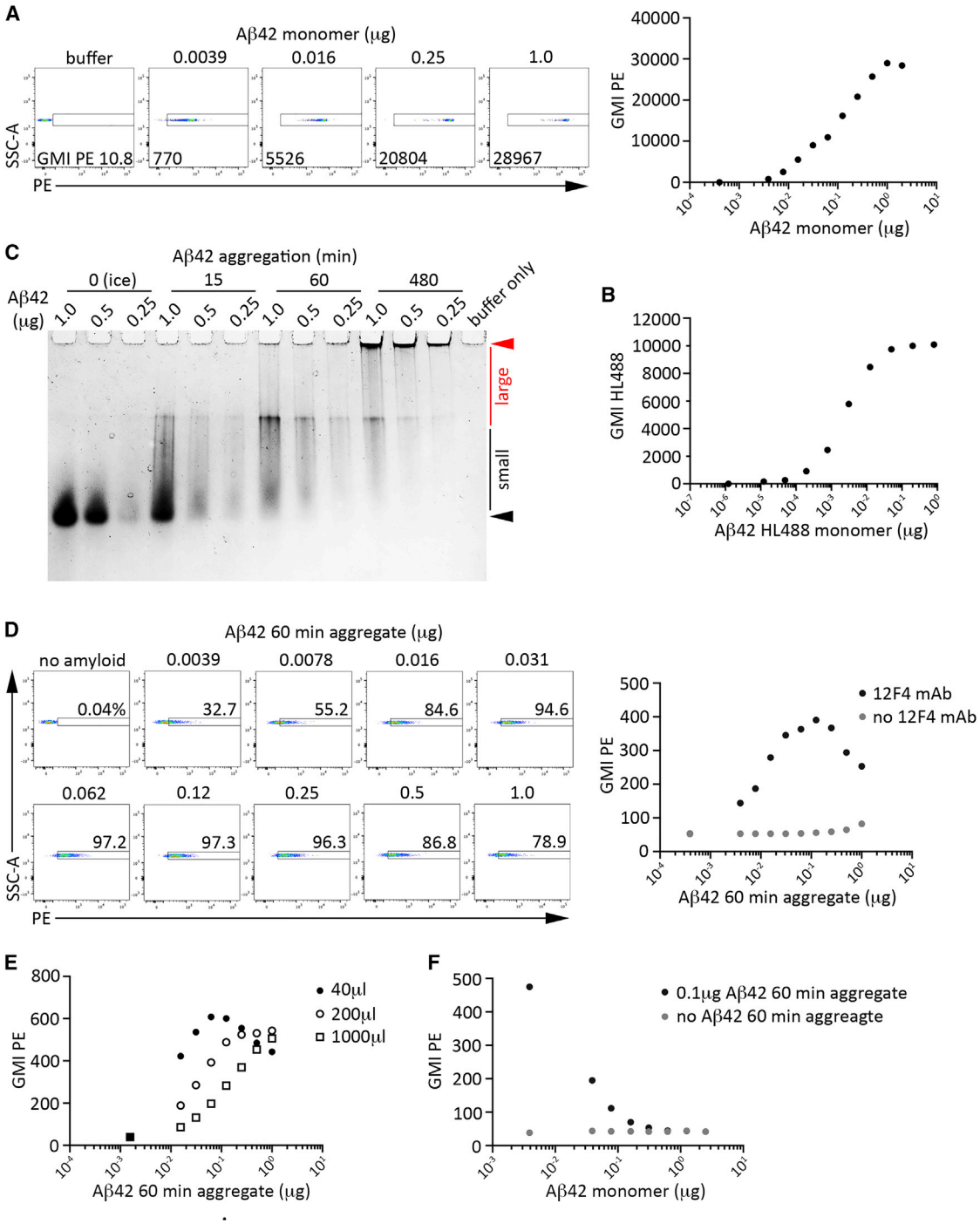

Figure 3. Determination of 12F4 mAb specificity and effective assay working conditions

(A) Lyophilized monomer Aβ42 was resuspended at 0.25 μg Aβ42/1.0 μL assay buffer A, titrated as indicated, incubated with 1.0 μL aldehyde sulfate beads (100 μL total volume buffer), and processed for detection by flow cytometry. Representative dot plots display both the PE^{+} bead gate and GMI PE for all beads. The graph displays the bead GMI for all Aβ42 titrations.

(B) Fluorescently labeled monomeric Aβ42 (Aβ42 HL488) titrated at the indicated amount was incubated with beads for 45 min to allow adsorption (0.1 μL bead stock/100 μL total volume), and the beads were subsequently analyzed by flow cytometry. The bead GMI HL488 is presented for all titrations.

(C) Aβ42 monomer solution was kept on ice (0 min), or incubated at 37°C/1,000 rpm for the time indicated (15, 60, 480 min) to induce multimerization. The resultant Aβ42 samples were prepared at the indicated amounts and resolved by native PAGE, stained, and imaged. Noted are the migrating distances of the stock monomer (black arrowhead), small multimers (black line), large multimers (red line), and large aggregates that failed to migrate (red arrowhead).

(legend continued on next page)

fluorescently conjugated Aβ42 (HL488 Aβ42) was adsorbed directly onto beads (Figure 3B), providing additional support that the fluorescence measured following 12F4 mAb-mediated detection in Figure 3A was in fact due to 12F4 mAb binding to Aβ42. We then used established experimental conditions, heat and agitation, to induce aggregation of monomeric Aβ42. Native PAGE of monomer solutions incubated for 15, 60, or 480 min at 37°C/1,000 rpm illustrated the comparative aggregation state of Aβ42 (Figure 3C). Monomeric Aβ42 was largely restricted to a single band; Aβ42 incubated for 15 and 60 min showed evidence of increasing aggregation into larger multimeric forms, whereas Aβ42 incubated for 480 min resulted in very large species that failed to enter the gel. The 60 min solution appeared to have the widest spectrum of Aβ42 multimeric species, small ranging to large, and thus was utilized for subsequent experiments. We first evaluated assay parameters that could result in a hooking effect, a commonly observed phenomenon in research and clinical ELISA-based assays where analyte concentrations above the assay hook point result in reduced signal intensity (Dodig, 2009; Erickson and Grenache, 2016; Jassam et al., 2006). Titrated 60 min Aβ42 material was incubated with beads lacking capture antibody, or with 12F4 mAb-loaded beads, followed by detection and flow cytometry analysis. We observed an increase in both the percentage of PE^+ beads and GMI PE as Aβ42 amount increased (range 0.0039 μg to approximately 0.1 μg); however, there was a marked decrease in bead fluorescence at higher levels of Aβ42 (Figure 3D). This indicated that the hook point was around 0.1 μg Aβ42/100 μL buffer. Control beads without capture antibody showed no to minimal fluorescence above background, indicating that 12F4 mAb-mediated Aβ42 capture was required for detection of antibody binding, and thus provided further confirmatory evidence for efficient bead blocking and antibody specificity. Increasing the reaction volume from 40 to 200–1,000 μL, thereby decreasing the analyte concentration, resulted in a shift of the fluorescence curve to the right (Figure 3E). This provided further evidence that Aβ42 binding and detection was dependent on Aβ42 concentration, and as a result we set 0.1 μg Aβ42/40–100 μL as an upper concentration limit to stay within the working detection range of the assay.

Using these assay parameters as a guide, we performed a competition experiment to determine if Aβ42 aggregate-to-bead binding could be blocked if incubation occurred in the presence of monomeric Aβ42. Equivalent 0.1 μg samples of 60 min Aβ42 aggregate were first combined with titrated monomer and then incubated with 12F4 mAb-loaded beads under standard conditions (60 min, room temperature). Detection and flow cytometry acquisition proceeded by standard methods as well. The data revealed that we could effectively compete 60 min Aβ42 aggregate binding with monomer levels greater than 1.0 μg, and that monomer at all tested amounts incubated without Aβ42 aggregates showed no appreciable fluorescence above background (Figure 3F). This indicated that the 12F4-Aβ42 interaction is specific, and that only higher-order Aβ42 multimers, not monomers, are detected by the assay.

Having established the bead-12F4 mAb conjugation amount, the effective assay blocking conditions, and the assay hook concentration, and having confirmed antibody specificity, we then evaluated assay reproducibility and sensitivity. Titrated solutions from the identical stock of Aβ42 aggregate were prepared every other day over 5 days and analyzed. Assay parameters and methods were stringently consistent. Our results indicated that bead GMI PE and percentage PE^+ beads were reproducible, as determined by the mean values across days (Figures 4A, 4B, and 4C). Notably, detection of aggregates above background was significant at sub-nanogram levels, indicating sensitivity on the scale of ELISA-based methods and immunoblot (Figures 4B and 4C [asterisks]).

To compare our results for bead assay quantitation of Aβ42 aggregates with commonly employed methods to measure protein aggregation, Aβ42 prepared at the above amounts was subjected to both native PAGE immunoblot and measurement of light scatter (turbidity). As expected, decreasing amounts of Aβ42 resulted in a reduced signal by anti-Aβ42 immunoblot (Figure 4D [left to right on each image]), which corresponded well to our results for the bead assay (Figure 4B). Although the detection limit was comparable for the two methods ($\sim 10^{-4}$ μg Aβ42), the quantitative linear range for detection by immunoblot was limited to approximately 4-fold Aβ42 (compare short exposure [left, 7 s] to long exposure [right, 12 min]). In contrast, there were quantifiable differences in signal intensity across the entire range of samples analyzed by the bead assay down to the detection limit. Furthermore, the time required to complete the bead assay, from start to data analysis, was less than 1 working day, compared with 2 days for immunoblot. When the identical Aβ42 amounts were analyzed for turbidity (spectrophotometry absorbance 395 nm [A395]), we were unable to detect any change in light scatter above background for all samples tested (Figure 4E). To confirm that our methodology to measure turbidity was sufficient, we analyzed uncoated microbeads over a large titration range. Our results showed an increase in A395 as the volume of beads in solution increased (Figure 4F), indicating that our system was in place to measure turbidity. In total, a comparison of the bead assay with immunoblot and turbidity measurement highlight sensitivity, quantitative range, and rapidity to assay completion as advantageous bead assay characteristics.

Bead assay detection of Aβ42 oligomers and protofibrils

Multiple studies indicate the form of an aggregate, whether small order multimers (oligomers), intermediate-sized protofibrils, or

(D) Beads activated with either 12F4 mAb or buffer only were blocked, incubated with the indicated amount of Aβ42 60 min multimers (100 μL total volume), and processed for detection by flow cytometry. Representative dot plots with the gated PE^+ population are shown. The graph displays the bead GMI PE for 12F4 mAb-activated beads (black) and buffer only beads (gray).
(E) 12F4 mAb-loaded beads were incubated with titrated Aβ42 60 min multimers in the indicated reaction volumes (solid black circle, 40 μL; open black circle, 200 μL; open black square, 1,000 μL), and processed for detection by flow cytometry. The graph displays the bead GMI PE of all beads.
(F) 12F4 mAb-activated beads were incubated with or without 0.1 μg Aβ42 60 min aggregates in the presence of the indicated amount of Aβ42 monomer, and processed for detection by flow cytometry. The bead PE GMI for beads incubated with (black) or without (gray) aggregate are presented.

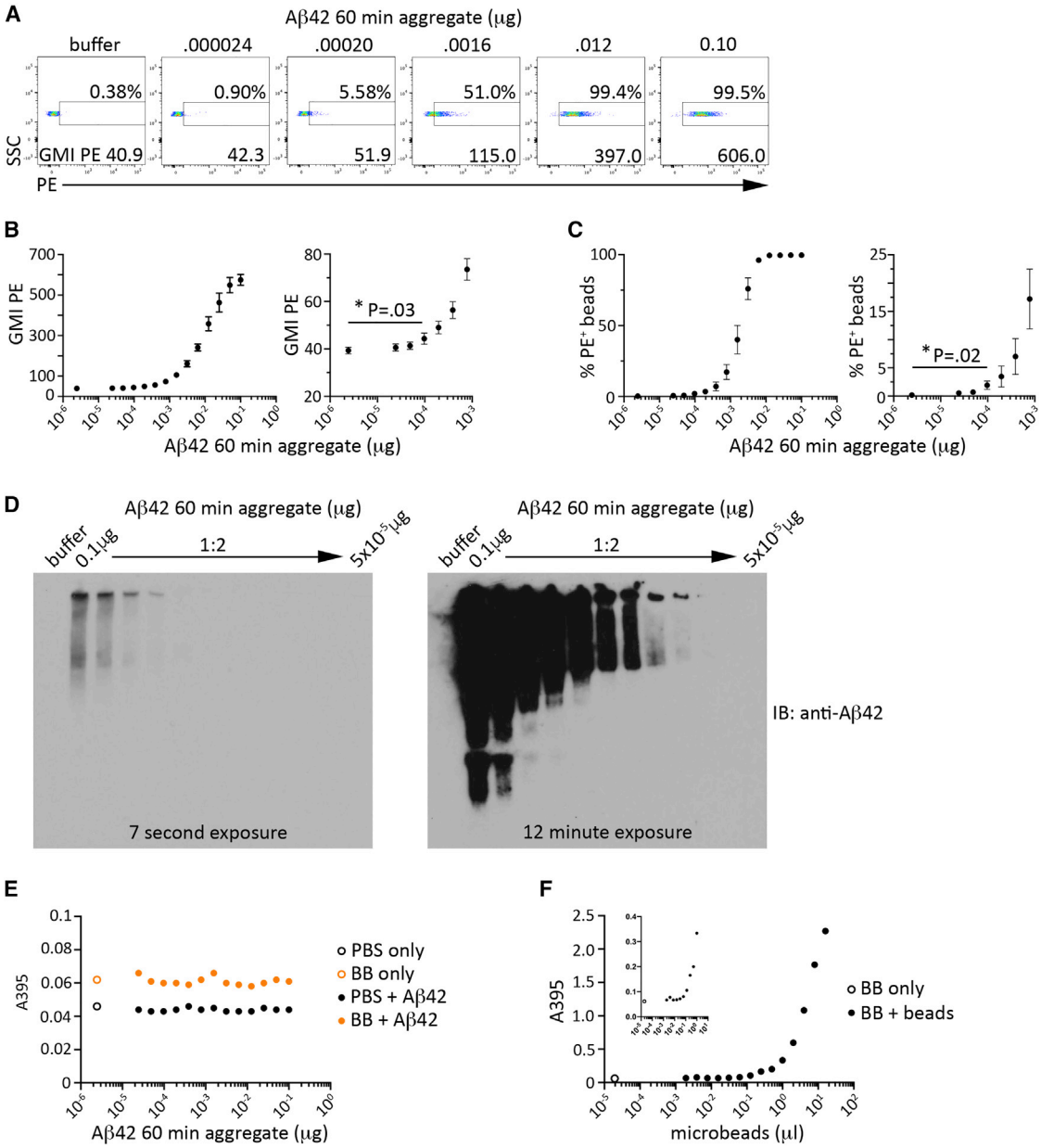

Figure 4. Assay sensitivity and comparison to other methods

(A) 12F4 mAb-activated beads were incubated with titrated Aβ42 60 min aggregate, followed by detection and flow cytometry analysis. The dot plots display representative examples of bead GMI PE and percentage of PE^+ beads (indicated by gate).

(B) The GMI PE for all titrations (left) and the most dilute samples only (right) are presented. The lowest Aβ42 amount that displayed significance compared with no amyloid control is indicated.

(C) The percentage PE^+ beads for all titrations (left) and the most dilute samples only (right) are presented. Indicated is the lowest Aβ42 amount that displayed significance compared with no amyloid control.

(D) Titrated Aβ42 60 min aggregate at the indicated amounts was resolved by native PAGE and immunoblot was performed using an anti-Aβ42 mAb. Representative images are presented for short (left, 7 s) and long (right, 12 min) film exposures.

(E) Titrated Aβ42 60 min aggregate was prepared in either PBS (black solid circles) or blocking buffer (BB) (orange solid circles) and analyzed by spectrophotometry at 395 nm. Open circles designate either PBS only (black) or BB only (orange) samples. Presented are the A395 measurements for the indicated amount of Aβ42.

(F) Aldehyde sulfate microbeads (4 μm diameter) were titrated in BB and analyzed by spectrophotometry at 395 nm. The A395 measurements for all titrated samples and most dilute samples only (inset graph) are presented. N = 3 for (A–C). Data presented in (E) and (F) are representative of at least two independent experiments. Errors bars indicate SD of the mean. *$p < 0.05$.

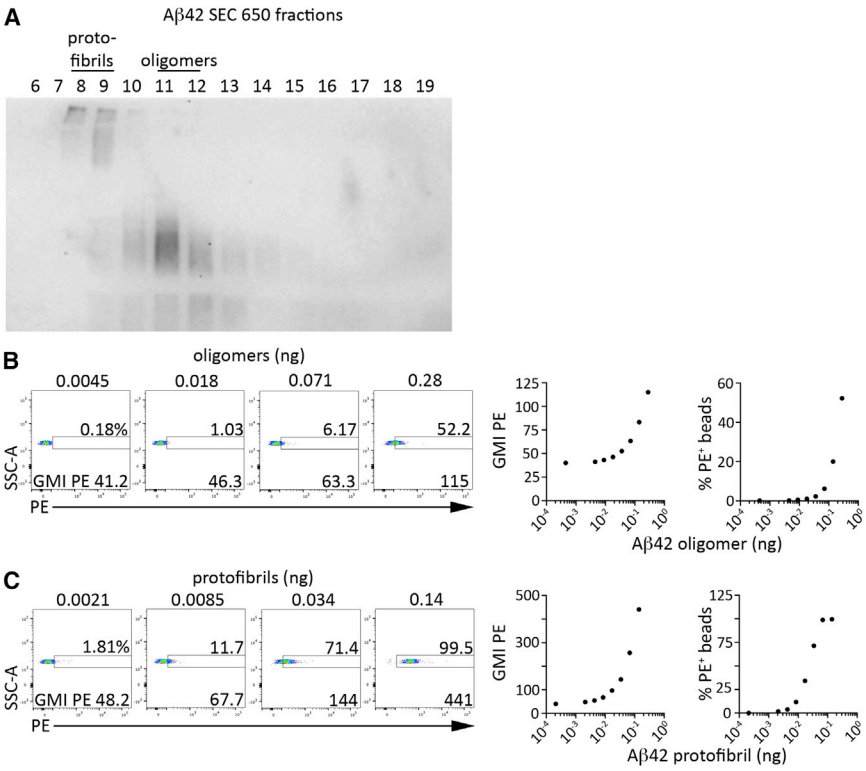

Figure 5. Assay detection of Aβ42 oligomers and protofibrils

(A) To isolate Aβ42 oligomers and protofibrils, Aβ42 monomers were incubated at 4°C for 120 h to induce multimerization, and the resultant samples were subjected to size-exclusion chromatography. Equivalent volumes of the indicated fractions were resolved by PAGE, stained, and imaged. Indicated are the fractions enriched for protofibrils (8,9) and oligomers (11,12).

(B) Pooled oligomer fractions were titrated at the indicated amounts and then analyzed by the bead assay. The PE^+ population and GMI PE of all beads for representative samples are indicated in the dot plots. The graphs display the GMI PE (left) and percentage of PE^+ beads (right) for all analyzed samples.

(C) Pooled protofibril fractions were titrated at the indicated amounts and then analyzed by the bead assay. The PE^+ population and GMI PE of all beads for representative samples are indicated in the dot plots. The graphs display the GMI PE (left) and percentage of PE^+ beads (right) for all analyzed samples.

large fibrils, may convey unique functional and pathophysiological consequences (Chen et al., 2017; Haass and Selkoe, 2007). To test the ability of the bead assay to detect Aβ42 oligomers or protofibrils specifically, we utilized established protocols to generate both species from Aβ42 monomers (Esparza et al., 2016; Ryan et al., 2010). Following size-exclusion chromatography, the collected samples were resolved by PAGE and, as expected, we observed fractions enriched for either protofibrils (slower migration; fractions 8,9) or oligomers (faster migration; fractions 11,12) (Figure 5A). The indicated fractions were then pooled, Aβ42 concentration was determined by ELISA method, and the samples were titrated and evaluated by the bead assay. Our results demonstrated that both oligomers (Figure 5B) and protofibrils (Figure 5C) could be detected above no amyloid control at sub-nanogram levels, in line with what was observed above for the Aβ42 60 min aggregate sample.

Bead assay characterization of Aβ42 multimer size

Current methods employed to study protein aggregation are qualitative to the presence of aggregation, but do not measure aggregate size. To address the utility of the bead assay for measurement of this parameter, solutions of monomeric Aβ42 were incubated with heat and agitation (37°C/1,000 rpm) for different periods of time. This standardized method, common for assays such as ThT, produces progressively higher-order multimers. Samples were harvested every 5 min for the first 30 min, and then at 45 and 60 min. Samples from each time point were resolved by native PAGE and displayed progressive transformation of majority monomeric Aβ42 at no incubation (0 min; black arrow) to a mix of smaller (black line) and larger (red line) multimers at 60 min, with some protein species being of such large size that they fail to migrate (red arrow) (Figure 6A). An equivalent amount of protein from each time point was then analyzed by the bead assay, with the PE positive bead population first established using the buffer only sample (no Aβ42). This population was then divided into four proportionally equivalent populations (quadrants) using the sample that displayed the highest overall fluorescence intensity (Figure 6B, 60 min aggregation time). Given that only multimers, and not monomers, can produce fluorescent beads above background levels, we could determine not only the percentage of beads that displayed positive fluorescence (multimer detection), but also the proportion of beads in each of the four populations based on relative bead PE intensity (1 PE^{dim}, 2 PE^{low}, 3 PE^{med}, 4 PE^{high}). Applied to all time points, the gating revealed that longer aggregation time resulted not only in more PE positive beads, but also proportionally brighter beads (Figure 6C). In particular, whereas between 45 and 60 min the increase in the amount of positive beads was small, the increase in PE^{high} beads was dramatic, from essentially no PE^{high} beads at 45 min to a quarter of all the beads at 60 min. This was accompanied by a marked decrease in the fraction of PE^{dim} beads. Moreover, the increase in positive beads with aggregation time corresponded with our observed increase in higher-order Aβ42 multimer species (Figure 6A). In addition, the most notable shift to brighter beads, at 45 and 60 min, is in line with the formation of the highest-order multimers at these time points as confirmed by native gel. These results demonstrate that the microparticle immunocapture assay reflects multimer size independently of multimer amount.

To further test this result indicating that larger aggregates produce brighter beads, we utilized centrifugation to isolate Aβ42 multimers based on sedimentation velocity (Mok and Howlett, 2006; Stine et al., 2003). Multimeric species were first generated

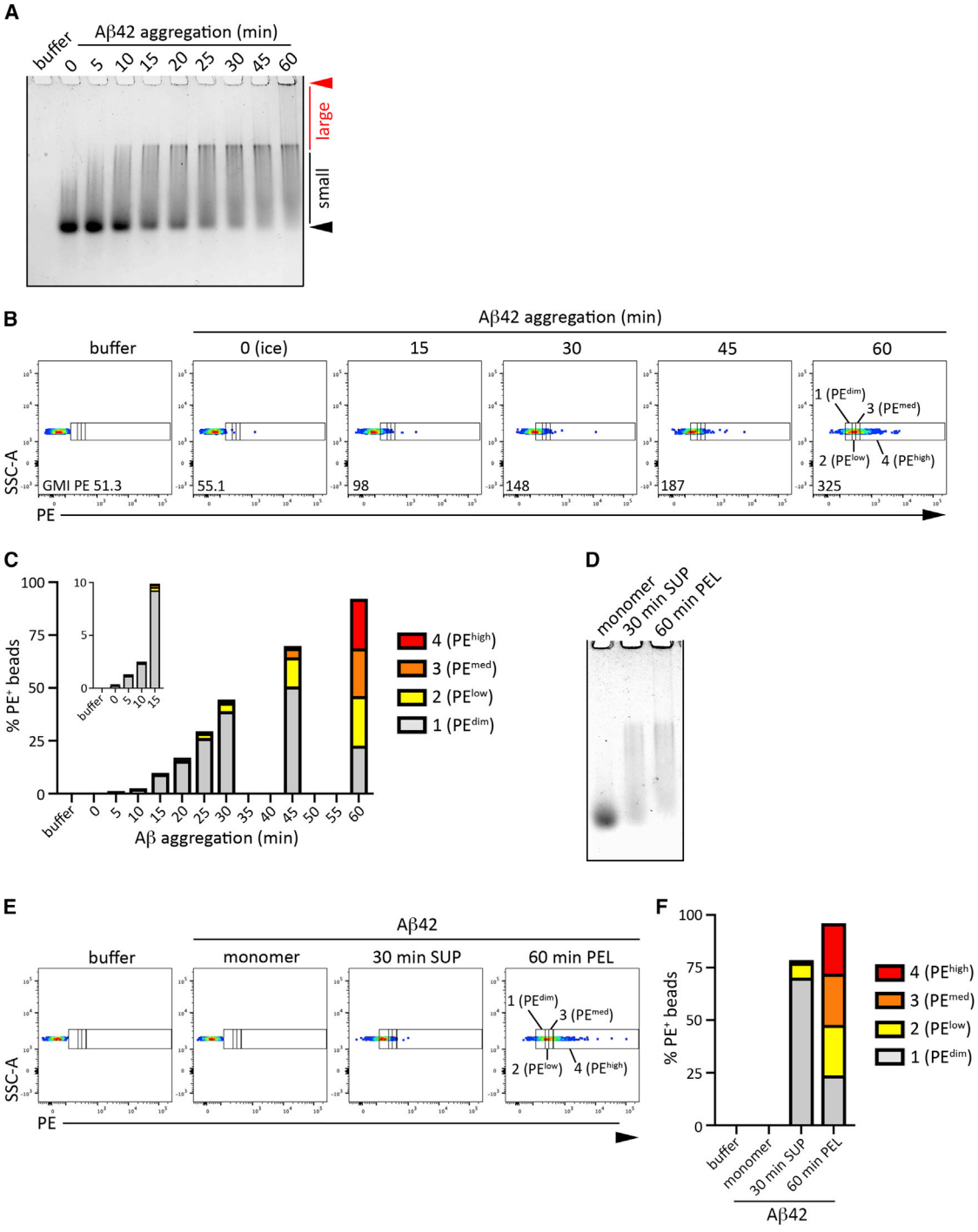

Figure 6. Quantitation of Aβ42 multimer size

(A) Aβ42 monomer solution was kept on ice (0 min) or incubated at 37°C/1,000 rpm for the indicated amount of time to induce aggregation. An equivalent amount of protein for each sample was resolved by native PAGE, stained, and imaged. Noted are the migrating distances of the stock monomer (black arrowhead), small multimers (black line), large multimers (red line), and large aggregates that failed to migrate (red arrowhead).

(B) Aldehyde sulfate beads were activated with 12F4 mAb, incubated with 0.1 μg of the Aβ42 preparations described above, and processed for detection by flow cytometry. Buffer only condition was used first to define PE^+ beads. The 60 min aggregate sample (rightmost dot plot) was used second to define four bead quadrants (equivalent proportions) based on relative PE fluorescence intensity. The gates were then applied to all samples and the percentage of beads in each of the four populations was determined. Dot plots for the indicated sample preparations are presented.

(legend continued on next page)

by incubation (37°C/1,000 rpm) for 30 or 60 min, followed by centrifugation to isolate comparatively larger (pelleted, 60 min PEL) and smaller (supernatant, 30 min SUP) protein species. Samples resolved by native PAGE exhibited the expected shift in migration when compared with Aβ42 monomer, with the 60 min PEL displaying reduced migration compared with 30 min SUP (Figure 6D). Application of the gating scheme described above for bead assay analysis revealed that, whereas the amount of PE positive beads in the 60 min PEL sample was only minimally increased compared with the 30 min SUP, the fraction of PE^{med} to PE^{high} beads was markedly increased (Figures 6E and 6F), and the fraction of PE^{dim} beads was markedly decreased. These results provide additional evidence that increased Aβ42 size is reflected in increased bead fluorescence. In total, these data suggest that the bead assay can measure not only the degree of protein multimerization but also distinguish multimers by size.

Detection of αS protein aggregates

To test the versatility of the microparticle immunocapture platform we examined aggregation-prone αS. We first acquired commercially available human wild-type monomeric αS and induced aggregation with heat and agitation according to the manufacturer's instructions. Resolved αS monomer samples by native PAGE revealed a predominant single band (Figure 7A, first four sample lanes). The presence of a higher-order species (red arrow), along with a reduction in amount of the faster migrating monomer species, indicated that the sample had undergone aggregation (last four lanes). To this point, our proof-of-concept approach for the bead assay had utilized Aβ42, so we next validated the critical bead assay characteristics of target specificity and aggregate only detection using αS. Beads activated with or without the anti-αS mAb MJFR1 were incubated with titrated αS monomer or αS aggregate samples and subsequently subjected to a similar block, wash, detection (here PE conjugated MJFR1), and flow acquisition protocol as utilized for the bead assays involving Aβ42. Prior experiments (data not shown) had revealed that the optimal mAb:bead conjugation ratio and αS amount were similar to those established for Aβ42, conditions that allowed for maximal bead intensity while staying below the hook point for the assay. Incubation of either αS monomer or αS aggregate with non-MJR1-activated beads resulted in bead fluorescence that was near background levels (Figure 7B, left side of graph). The same was true for MJFR1-activated beads incubated with αS monomer. However, incubation of activated beads with αS aggregate samples produced markedly brighter beads whose fluorescence intensity increased with increasing levels of αS (Figure 7B, right side of graph). These results indicated that the MJFR1-conjugated bead assay platform was specific for aggregated αS only and could measure the amount of aggregated αS.

Detection of αS protein aggregates in human CSF

There is much interest in the detection and measurement of protein aggregates in biological specimens. However, although simple in concept, the ability to detect protein species in biological matrices is often compromised to some degree by yet uncharacterized factors present in the matrix that do not exist in standard, controlled laboratory buffers and solutions, for which reason it is often recommended to test biological fluids at 1% concentration (DeForge et al., 2007; Lachno et al., 2015; Mollenhauer et al., 2008). We therefore tested the utility of the bead assay in detection of aggregated αS in human CSF specimens. Equivalent amounts of monomeric αS prepared in buffer alone or in buffer with titrated CSF, incubated with MJFR1-activated beads, and subsequently analyzed by flow cytometry produced bead intensities with similar background (Figure 7C, left side of graph). With aggregated αS, we observed a progressive decrease in bead fluorescence compared with buffer alone as the amount of CSF increased (0.4%–25% CSF); however, even at 25% the signal intensity was well above background (GMI PE 47.6 versus 1,452). These results showed that, although we did observe a matrix influence on αS detection, we could detect aggregated αS, but not monomeric αS, in a physiologically and pathologically relevant biological material. Building from these results, we then determined the limits of detection of aggregated αS in CSF. Titrated αS aggregate was prepared in either buffer or buffer + 1% CSF and analyzed by the bead assay. Flow cytometry dot plots show a comparable bead fluorescence profile (spread) and PE intensity (GMI) for buffer (top row) and buffer/CSF (bottom row) samples (Figure S1; GMI in lower left of plot). Data from four independent assays indicated equivalent fluorescence values for the two buffer conditions across all tested samples (Figure 7D, inset graph low αS levels only). Furthermore, we observed a significant difference in PE intensity above background for both conditions at approximately 4.9×10^{-5} μg αS (GMI PE: buffer 44.2 versus 51.9, buffer/CSF 45.2 versus 51.1). Thus, the microparticle immunocapture assay represents a platform that can be readily adapted to detect other species of protein aggregates, in this case αS, and can do so in a biological fluid (CSF).

To this point, validation and application of the assay involved CSF from normal human donors spiked with aggregated αS prepared *in vitro* under experimentally controlled conditions. Given the potential significance of establishing the microparticle platform as a methodological tool for aggregate quantitation in

(C) The percentage of beads in each population, designated in silver (PE^{dim}), yellow (PE^{low}), orange (PE^{med}), and red (PE^{high}), are presented. Data for the shortest aggregation time only (0–15 min) are shown in the inset graph.
(D) Aβ42 monomers were incubated for 30 or 60 min at 37°C/1,000 rpm and then subjected to ultracentrifugation. Equivalent Aβ42 amount from the 30 min supernatant (30 min SUP), the 60 min pellet (60 min PEL), and Aβ42 monomer were resolved by native PAGE, stained, and imaged.
(E) Beads were activated with 12F4 mAb, incubated with 0.1 μg of the Aβ42 preparations described above, and processed for detection by flow cytometry. A gating scheme similar to that described above was applied. Here, the 60 min PEL PE^{+} bead population was utilized to derive four quadrants, and the gates were then applied to all samples. Displayed are the dot plots with applied gates.
(F) The graph displays the percentage of beads in each population, designated by color as above. Note: data presented for the aggregation time course (A–C) and the isolation of Aβ42 species by differential ultracentrifugation (D–F) are representative of at least two independent experiments.

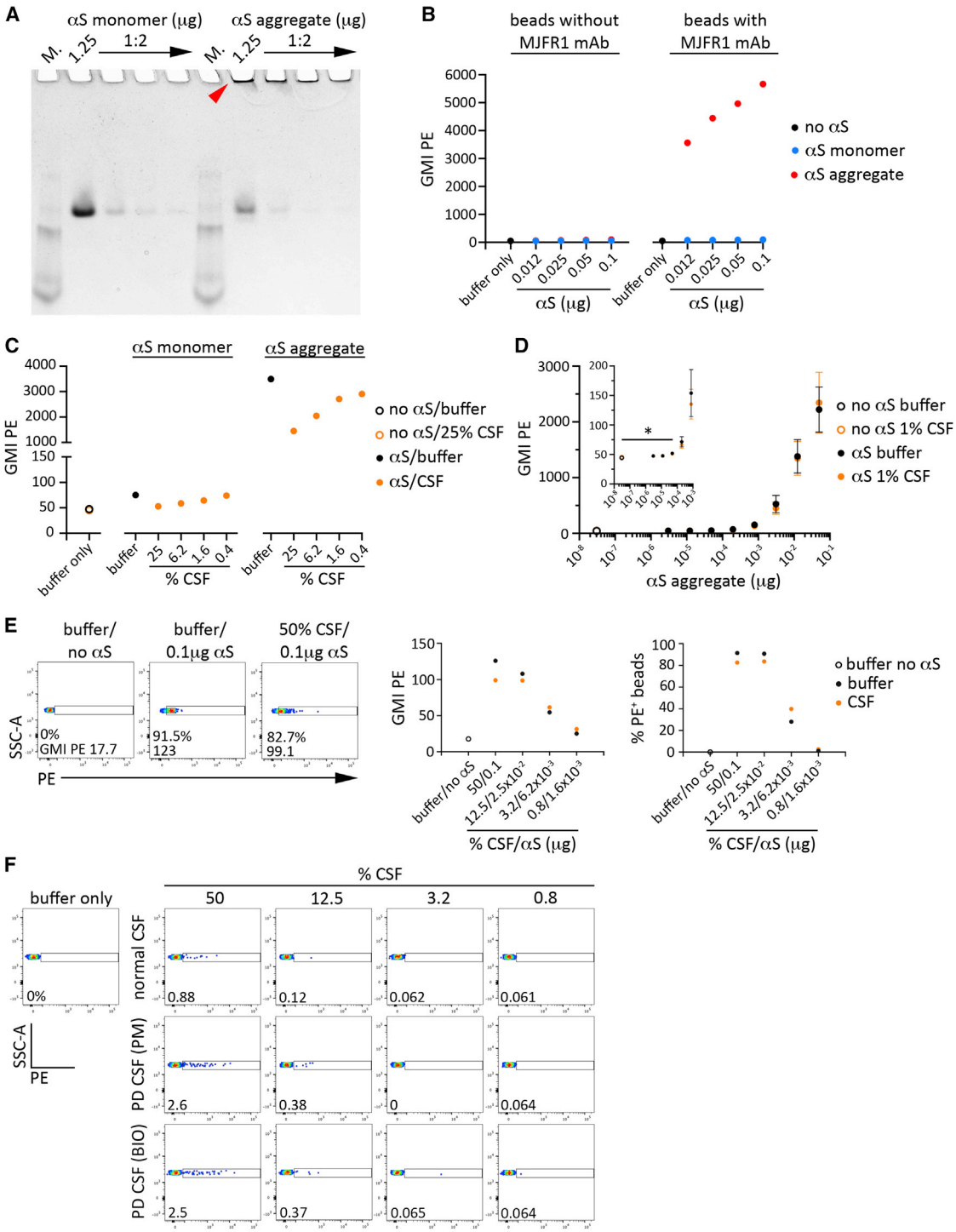

Figure 7. Detection and measurement of aggregated alpha-synuclein (αS) in human cerebrospinal fluid (CSF)

(A) Monomeric αS was aggregated according to the manufacturer's instructions (37°C/1,000 rpm) and analyzed by native PAGE to confirm aggregation state. Displayed are titrated (starting 1.25 μg αS, with 1:2 dilutions) αS monomer (left lanes) and αS aggregate (right lanes). Use of protein molecular weight standards (indicated M, lanes 1 and 6) is for the purposes of sample lane separation and gel orientation only and not to determine sample molecular weight. The red arrowhead indicates the accumulation of aggregated protein in the αS aggregate sample, which is not visible in the αS monomer sample.

(B) Aldehyde sulfate beads were incubated in either PBS alone or PBS + anti-αS mAb MJFR1, and subsequently blocked, washed, and incubated with titrated αS monomer or αS aggregate. Following detection with MJFR1-PE mAb, the beads were analyzed for PE intensity by flow cytometry. The graph displays the GMI PE

(legend continued on next page)

diseased individuals, we next assessed how the assay would perform on CSF collected from Parkinson's disease (PD) patients. Our analysis of aggregated αS added to normal CSF, and then titrated in buffer, indicated that optimal detection occurred when the samples in CSF were less dilute (left and right graphs, orange dots); however, bead fluorescence was most near buffer conditions (black dots) as the dilution increased (Figure 7E). This was in line with our results using equivalent αS amount in titrated CSF (see Figure 7C). Using similar parameters to analyze PD CSF samples for the presence of aggregated αS, we observed a distinct population of PE^+ beads in both evaluated PD CSF samples that decreased with sample titration (Figure 7F, rows two and three, gated population). Notably, the populations displayed a relatively broad fluorescence pattern (compare with Figure 7E dot plot, third column), indicating the existence of higher-order aggregates, which, as expected, were approximately 3- to 4-fold greater in number than that detected in normal CSF (column one, 2.6% and 2.5% versus 0.88% at 50% CSF; column two, 0.38% and 0.37% versus 0.12% at 12.5% CSF) (Shahnawaz et al., 2020). These results indicate that the bead assay cannot only detect naturally generated aggregated αS in CSF, but also suggest assay utility for comparative quantitative analyses across multiple patient samples.

DISCUSSION

Maintenance of protein homeostasis (proteostasis) is essential for cellular and organismal health. Given the strong experimental and observational evidence connecting protein aggregation with neurodegenerative and other diseases, methodologies to assess protein aggregation have been developed and relied upon by basic science and clinical investigators. There are, however, substantial deficiencies in the repertoire of the tests presently available that hinder a more complete analysis of protein aggregation. In particular, measurement of multimer size has been lacking. Herein we present a bead fluorescence assay to detect protein aggregates that uses highly quantitative flow cytometry analysis to discriminate protein monomers from multimeric species and characterize the degree of protein multimerization.

At the core of our design is a microparticle immunocapture platform, in which a monoclonal capture antibody is adsorbed onto super active aldehyde sulfate beads, followed by sample incubation and capture, detection antibody incubation, and flow cytometry analysis. In theory, target protein binding to the capture mAb will saturate all available antibody binding sites on a monomeric target and thus prohibit any subsequent binding of a detection antibody fashioned from a mAb identical to the capture mAb. Multimer capture will occur by the same process; however, sites will remain unoccupied and thus open to binding by the detection mAb, with the number of unoccupied sites proportional to the number of individual units that comprise the multimer. Our results demonstrate that this did in fact occur, for both tested proteins Aβ42 and αS, thus indicating not only protein-specific multimer detection but a high level of adaptability in terms of aggregation-prone proteins for which suitable antibody reagents exist. An additional advantageous feature is the short duration required to complete the assay, as data could be generated for a sample set, from start to finish, in less than one working day. Although turbidity measurements provide a rapid result, they cannot compare with microparticle immunocapture platform in terms of sensitivity and provide no information regarding size.

A limitation of several other commonly utilized assays, including ThT and plate-based ELISA (El-Agnaf et al., 2000, 2006; Gade Malmos et al., 2017), is that signal intensity reflects only the overall degree of aggregation for a sample, while differences in size of individual aggregates that comprise the total are not detected or quantified. Although quantitation of total aggregation is informative and valuable, there is mounting evidence that aggregate size, small oligomer versus protofibril versus fibril, has biological significance. Size analysis by immunoblot, EM, or gel filtration chromatography (GFC) can be informative, but application may be limited due to practical considerations for immunoblot and EM, and the limited size range for GFC. We suggest that the inherent characteristics of the bead platform provide substantial advantages. A bead that has captured in proportion more larger aggregates will fluoresce more than a bead with smaller

of beads without mAb activation (left) or with MJFR1 mAb activation (right) for all titrated samples of αS monomer (blue circles) and αS aggregate (red circles), or no αS (buffer, black circles).

(C) Human CSF was prepared at the indicated concentration in PBS (25.0%–0.4% CSF) and spiked with an equivalent amount (0.5 μg) of either αS monomer or αS aggregate. The samples were then incubated with MJFR1-activated beads, and processed for detection by flow cytometry. The graph displays the GMI PE for all beads analyzed for each condition. Open circles indicate samples prepared without αS in either buffer alone (black) or 25% CSF (orange; overlaps with open black circle). Indicated by solid circles are buffer alone + αS (black), or titrated CSF + αS (orange).

(D) Aggregated αS was titrated at the indicated amount and combined with 1% human CSF. Following incubation with MJFR1 mAb-activated beads, the samples were processed for detection by flow cytometry. The graph displays the bead GMI PE for all titrated samples. Open circles represent samples prepared without αS in either buffer alone (black) or 1% CSF (orange; overlaps with open black circle). Depicted by solid circles are buffer alone + αS (black) or 1% CSF + αS (orange). The inset graph displays the most dilute αS preparations only. Indicated is the αS amount at which a statistically significant difference in PE intensity above buffer alone conditions was observed.

(E) Aggregated αS was prepared at 0.1 μg in either buffer or 50% CSF/buffer. The samples were then titrated 1:4 in buffer and subsequently analyzed by the bead assay. Indicated by dot plot are the percentage of PE^+ beads and GMI PE for buffer/no αS (column one), buffer/0.1 μg αS (column two), and 50% CSF/0.1 μg αS (column three) conditions. The graphs display the GMI PE intensity (left) and the percentage of PE^+ beads (right) at the indicated αS amount for buffer (black) and CSF (orange) conditions. The open black circles represent buffer only conditions with no αS added.

(F) Parkinson's disease patient CSF (PD CSF) and normal CSF were titrated in buffer at the indicated amount and analyzed by the bead assay. The gated populations indicate the percentage of PE^+ beads at each titration as compared with buffer only conditions (far left dot plot). Note: data presented in (B) and (C) are representative of at least two independent experiments. For (D), N = 4 independent experiments from four separate human CSF donors. Errors bars indicate SEM. *$p < 0.05$.

See also Figure S1.

aggregates due to a greater number of available detection mAb binding epitopes. Thus, sample solutions that have a greater proportion of large aggregates to small aggregates will generate beads that display higher fluorescence. This is clearly shown by flow cytometry dot plot analysis in Figure 6, where four equivalent quadrants were constructed for the fluorescence profile of the sample that displayed the highest overall PE intensity (60 min aggregation) and then applied to all samples. Although the total number of PE^+ beads varied (increasing in number with aggregation time, see Figure 6C), it would be expected that, if aggregate size had no influence on bead fluorescence, then the proportion of beads in each of the four populations would be about one-quarter across all samples. This was not the case, as only at the later time points (30, 45, 60 min) were bead populations that are medium to high fluorescence observed. The bead assay showed similar size discrimination for protein aggregates separated by centrifugation. This type of analysis can be utilized with any sample set, and population gates can be set based on criteria established by the investigator. Furthermore, flow cytometry allows equal application of these gates across all samples, thus insuring that characterization of aggregate size based on bead fluorescence will be unbiased.

Although we foresee a large opening in basic science research and pharmaceutical quality control that can be filled with application of the bead assay, clinical research interests commonly lie in protein aggregate detection in human biological samples. Our experiments utilizing αS were designed to demonstrate the feasibility in a routinely analyzed human tissue, CSF, and detection of aggregated αS in CSF from PD patients provides additional support for use of the assay in a clinical context. In either investigative context, sample manipulation during the course of the assay is limited and thus the potential introduction of artifacts is lessened. It is specific (antibody-mediated detection), rapid (same day results), quantitative (flow cytometry readout), and readily adaptable to detect other species. Furthermore, and perhaps most notably, aggregates can be distinguished based on size. Given these attributes, we suggest that the assay possesses distinct advantages beyond the traditional methods of evaluation available up to now.

Limitations of the study

An essential component of the assay is the mAb required for capture and detection, and thus selection of which mAb to use is a critical first step. Our approach was to start with well-validated mAb that have an extensive record in the literature, and we propose that the binding, detection, and blocking experiments, as described in Figures 2 and 3, provide an appropriate guide to determine if a given antibody is a suitable candidate. We note that numerous experiments were completed to establish mAb:bead ratios and incubation conditions that offered an acceptable balance to minimize reagent requirements, enhance protein capture efficiency, generate maximal fluorescence signal intensity, and optimize flow cytometry acquisition parameters. Therefore, it is recommended that consideration be given to these points for all experimental designs, particularly when the assay is utilized to interrogate aggregation state in biological matrices, given the aforementioned technical issues that can arise in ELISA-based approaches under these conditions. It also became apparent early in our studies that protein (analyte) amounts above a certain concentration resulted in decreased bead fluorescence as the amount of protein increased. The fluorescence intensity curves display characteristics of the hook effect, a common feature to immunological assays that is attributed to excess analyte or antibody in solution (Dodig, 2009; Erickson and Grenache, 2016; Jassam et al., 2006). The observed hook point was very consistent, and could be manipulated with changes to protein concentration. Identification of the hook point can be achieved by a simple dilution, and would need to be completed for any tested protein. Although microparticle immunocapture successfully assessed αS aggregates added to human CSF, and endogenous αS aggregates in CSF from PD patients, continued study of a larger number of PD patient specimens will be needed to verify clinical utility.

STAR★METHODS

Detailed methods are provided in the online version of this paper and include the following:

- KEY RESOURCES TABLE
- RESOURCE AVAILABILITY
  - Lead contact
  - Materials availability
  - Data and code availability
- EXPERIMENTAL MODEL AND SUBJECT DATA
  - Mouse model
  - Human cerebrospinal fluid
- METHOD DETAILS
  - Mouse splenic B cells
  - Conjugation of antibody to aldehyde sulfate beads
  - Preparation of Aβ42 multimers
  - Binding of Aβ42 to 12F4 mAb-activated aldehyde sulfate beads
  - Detection of bead-captured Aβ42
  - Flow cytometry acquisition and analysis
  - Microscopy imaging of aldehyde sulfate beads and B cell isolation
  - Isolation of Aβ42 multimers by centrifugation
  - Native polyacrylamide gel electrophoresis (PAGE) and immunoblot
  - Spectrophotometry (turbidity) measurements
  - Purification of Aβ42 oligomers and protofibrils by size exclusion chromatography
  - Alpha synuclein aggregate formation and bead assay detection in human cerebrospinal fluid
- QUANTIFICATION AND STATISTICAL ANALYSIS

SUPPLEMENTAL INFORMATION

Supplemental information can be found online at https://doi.org/10.1016/j.crmeth.2022.100214.

ACKNOWLEDGMENTS

The authors would like to acknowledge the flow cytometry core facility at WMED and thank the core manager Michael Clemente for the means and assistance to complete the final, and essential, step of the assay. We would

also like to thank the members of our lab for constructive thought and feedback throughout the development of the methodology described herein. We are grateful for the funding to complete our work that was provided by NIH R01 AI142004, along with the institutional support from Western Michigan University Homer Stryker M.D. School of Medicine.

AUTHOR CONTRIBUTIONS

Conceptualization, M.F.G. and T.L.R.; methodology, M.F.G. and T.L.R.; investigation, M.F.G.; visualization, M.F.G.; writing – original draft, M.F.G. and T.L.R.; writing – review & editing, M.F.G. and T.L.R.; funding acquisition, T.L.R.; resources, H.K.; supervision, T.L.R.

DECLARATION OF INTERESTS

The authors declare no competing interests.

Received: April 15, 2021
Revised: December 13, 2021
Accepted: April 19, 2022
Published: May 23, 2022

REFERENCES

Aguzzi, A., and O'Connor, T. (2010). Protein aggregation diseases: pathogenicity and therapeutic perspectives. Nat. Rev. Drug Discov. *9*, 237–248. https://doi.org/10.1038/nrd3050.

Bagriantsev, S.N., Kushnirov, V.V., and Liebman, S.W. (2006). Analysis of amyloid aggregates using agarose gel electrophoresis. Methods Enzymol. *412*, 33–48. https://doi.org/10.1016/s0076-6879(06)12003-0.

Butler, J.E. (2000). Solid supports in enzyme-linked immunosorbent assay and other solid-phase immunoassays. Methods *22*, 4–23. https://doi.org/10.1006/meth.2000.1031.

Chaudhuri, R., Cheng, Y., Middaugh, C.R., and Volkin, D.B. (2014). High-throughput biophysical analysis of protein therapeutics to examine interrelationships between aggregate formation and conformational stability. AAPS J. *16*, 48–64. https://doi.org/10.1208/s12248-013-9539-6.

Chen, G.F., Xu, T.H., Yan, Y., Zhou, Y.R., Jiang, Y., Melcher, K., and Xu, H.E. (2017). Amyloid beta: structure, biology and structure-based therapeutic development. Acta Pharmacol. Sin. *38*, 1205–1235. https://doi.org/10.1038/aps.2017.28.

Cheng, Q., Danao, J., Talreja, S., Wen, P., Yin, J., Sun, N., Li, C.M., Chui, D., Tran, D., Koirala, S., et al. (2018). TREM2-activating antibodies abrogate the negative pleiotropic effects of the Alzheimer's disease variant *Trem2*^{R47H} on murine myeloid cell function. J. Biol. Chem. *293*, 12620–12633. https://doi.org/10.1074/jbc.ra118.001848.

Cox, D., Raeburn, C., Sui, X., and Hatters, D.M. (2020). Protein aggregation in cell biology: an aggregomics perspective of health and disease. Semin. Cell Dev. *99*, 40–54. https://doi.org/10.1016/j.semcdb.2018.05.003.

DeForge, L.E., Shih, D.H., Kennedy, D., Totpal, K., Chuntharapai, A., Bennett, G.L., Drummond, J.H., Siguenza, P., and Wong, W.L.T. (2007). Species-dependent serum interference in a sandwich ELISA for Apo2L/TRAIL. J. Immunol. Methods *320*, 58–69. https://doi.org/10.1016/j.jim.2006.12.001.

den Engelsman, J., Garidel, P., Smulders, R., Koll, H., Smith, B., Bassarab, S., Seidl, A., Hainzl, O., and Jiskoot, W. (2011). Strategies for the assessment of protein aggregates in pharmaceutical biotech product development. Pharm. Res. *28*, 920–933. https://doi.org/10.1007/s11095-010-0297-1.

Dodig, S. (2009). Interferences in quantitative immunochemical methods. Biochem. Med. *19*, 50–62. https://doi.org/10.11613/bm.2009.005.

El-Agnaf, O.M., Mahil, D.S., Patel, B.P., and Austen, B.M. (2000). Oligomerization and toxicity of beta-amyloid-42 implicated in Alzheimer's disease. Biochem. Biophys. Res. Commun. *273*, 1003–1007. https://doi.org/10.1006/bbrc.2000.3051.

El-Agnaf, O.M.A., Salem, S.A., Paleologou, K.E., Curran, M.D., Gibson, M.J., Court, J.A., Schlossmacher, M.G., and Allsop, D. (2006). Detection of oligomeric forms of alpha-synuclein protein in human plasma as a potential biomarker for Parkinson's disease. FASEB J. *20*, 419–425. https://doi.org/10.1096/fj.03-1449com.

Erickson, J.A., and Grenache, D.G. (2016). A chromogranin A ELISA absent of an apparent high-dose hook effect observed in other chromogranin A ELISAs. Clin. Chim. Acta. *452*, 120–123. https://doi.org/10.1016/j.cca.2015.11.007.

Esparza, T.J., Wildburger, N.C., Jiang, H., Gangolli, M., Cairns, N.J., Bateman, R.J., and Brody, D.L. (2016). Soluble amyloid-beta aggregates from human Alzheimer's disease brains. Sci. Rep. *6*, 38187. https://doi.org/10.1038/srep38187.

Gade Malmos, K., Blancas-Mejia, L.M., Weber, B., Buchner, J., Ramirez-Alvarado, M., Naiki, H., and Otzen, D. (2017). ThT 101: a primer on the use of thioflavin T to investigate amyloid formation. Amyloid *24*, 1–16. https://doi.org/10.1080/13506129.2017.1304905.

Haass, C., and Selkoe, D.J. (2007). Soluble protein oligomers in neurodegeneration: lessons from the Alzheimer's amyloid beta-peptide. Nat. Rev. Mol. Cell Biol. *8*, 101–112. https://doi.org/10.1038/nrm2101.

Jassam, N., Jones, C.M., Briscoe, T., and Horner, J.H. (2006). The hook effect: a need for constant vigilance. Ann. Clin. Biochem. *43*, 314–317. https://doi.org/10.1258/000456306777695726.

Lachno, D.R., Evert, B.A., Maloney, K., Willis, B.A., Talbot, J.A., Vandijck, M., and Dean, R.A. (2015). Validation and clinical utility of ELISA methods for quantification of amyloid-β peptides in cerebrospinal fluid specimens from Alzheimer's disease studies. J. Alzheimers Dis. *45*, 527–542. https://doi.org/10.3233/jad-141686.

Lindquist, S.L., and Kelly, J.W. (2011). Chemical and biological approaches for adapting proteostasis to ameliorate protein misfolding and aggregation diseases: progress and prognosis. Cold Spring Harb. Perspect. Biol. *3*, a004507. https://doi.org/10.1101/cshperspect.a004507.

Mahler, H.C., Friess, W., Grauschopf, U., and Kiese, S. (2009). Protein aggregation: pathways, induction factors and analysis. J. Pharm. Sci. *98*, 2909–2934. https://doi.org/10.1002/jps.21566.

Mendt, M., Kamerkar, S., Sugimoto, H., McAndrews, K.M., Wu, C.C., Gagea, M., Yang, S., Blanko, E.V.R., Peng, Q., Ma, X., et al. (2018). Generation and testing of clinical-grade exosomes for pancreatic cancer. JCI Insight *3*, e99263. https://doi.org/10.1172/jci.insight.99263.

Mogk, A., Bukau, B., and Kampinga, H.H. (2018). Cellular handling of protein aggregates by disaggregation machines. Mol. Cell *69*, 214–226. https://doi.org/10.1016/j.molcel.2018.01.004.

Mok, Y.F., and Howlett, G.J. (2006). Sedimentation velocity analysis of amyloid oligomers and fibrils. Methods Enzymol. *413*, 199–217. https://doi.org/10.1016/s0076-6879(06)13011-6.

Mollenhauer, B., Cullen, V., Kahn, I., Krastins, B., Outeiro, T.F., Pepivani, I., Ng, J., Schulz-Schaeffer, W., Kretzschmar, H.A., McLean, P.J., et al. (2008). Direct quantification of CSF alpha-synuclein by ELISA and first cross-sectional study in patients with neurodegeneration. Exp. Neurol. *213*, 315–325. https://doi.org/10.1016/j.expneurol.2008.06.004.

O'Brien, R.J., and Wong, P.C. (2011). Amyloid precursor protein processing and Alzheimer's disease. Annu. Rev. Neurosci. *34*, 185–204. https://doi.org/10.1146/annurev-neuro-061010-113613.

Palmqvist, S., Janelidze, S., Quiroz, Y.T., Zetterberg, H., Lopera, F., Stomrud, E., Su, Y., Chen, Y., Serrano, G.E., Leuzy, A., et al. (2020). Discriminative accuracy of plasma phospho-tau217 for Alzheimer disease vs other neurodegenerative disorders. JAMA *324*, 772–781. https://doi.org/10.1001/jama.2020.12134.

Polinski, N.K., Volpicelli-Daley, L.A., Sortwell, C.E., Luk, K.C., Cremades, N., Gottler, L.M., Froula, J., Duffy, M.F., Lee, V.M.Y., Martinez, T.N., and Dave, K.D. (2018). Best practices for generating and using alpha-synuclein pre-formed fibrils to model Parkinson's disease in rodents. J. Parkinsons Dis. *8*, 303–322. https://doi.org/10.3233/jpd-171248.

Ryan, D.A., Narrow, W.C., Federoff, H.J., and Bowers, W.J. (2010). An improved method for generating consistent soluble amyloid-beta oligomer preparations for in vitro neurotoxicity studies. J. Neurosci. Methods *190*, 171–179. https://doi.org/10.1016/j.jneumeth.2010.05.001.

Shahnawaz, M., Tokuda, T., Waragai, M., Mendez, N., Ishii, R., Trenkwalder, C., Mollenhauer, B., and Soto, C. (2017). Development of a biochemical diagnosis of Parkinson disease by detection of α-synuclein misfolded aggregates in cerebrospinal fluid. JAMA Neurol. *74*, 163–172. https://doi.org/10.1001/jamaneurol.2016.4547.

Shahnawaz, M., Mukherjee, A., Pritzkow, S., Mendez, N., Rabadia, P., Liu, X., Hu, B., Schmeichel, A., Singer, W., Wu, G., et al. (2020). Discriminating α-synuclein strains in Parkinson's disease and multiple system atrophy. Nature *578*, 273–277. https://doi.org/10.1038/s41586-020-1984-7.

Stine, W.B., Jr., Dahlgren, K.N., Krafft, G.A., and LaDu, M.J. (2003). In vitro characterization of conditions for amyloid-beta peptide oligomerization and fibrillogenesis. J. Biol. Chem. *278*, 11612–11622. https://doi.org/10.1074/jbc.m210207200.

Suárez, H., Gámez-Valero, A., Reyes, R., López-Martín, S., Rodríguez, M.J., Carrascosa, J.L., Cabañas, C., Borràs, F.E., and Yáñez-Mó, M. (2017). A bead-assisted flow cytometry method for the semi-quantitative analysis of Extracellular Vesicles. Sci. Rep. *7*, 11271. https://doi.org/10.1038/s41598-017-11249-2.

Tanaka, K., and Matsuda, N. (2014). Proteostasis and neurodegeneration: the roles of proteasomal degradation and autophagy. Biochim. Biophys. Acta *1843*, 197–204. https://doi.org/10.1016/j.bbamcr.2013.03.012.

Théry, C., Amigorena, S., Raposo, G., and Clayton, A. (2006). Isolation and characterization of exosomes from cell culture supernatants and biological fluids. Curr. Protoc. Cell Biol. *3*, 3.22. https://doi.org/10.1002/0471143030.cb0322s30.

Tokuda, T., Qureshi, M.M., Ardah, M.T., Varghese, S., Shehab, S.A.S., Kasai, T., Ishigami, N., Tamaoka, A., Nakagawa, M., and El-Agnaf, O.M.A. (2010). Detection of elevated levels of α-synuclein oligomers in CSF from patients with Parkinson disease. Neurology *75*, 1766–1770. https://doi.org/10.1212/wnl.0b013e3181fd613b.

Vogler, E.A. (2012). Protein adsorption in three dimensions. Biomaterials *33*, 1201–1237. https://doi.org/10.1016/j.biomaterials.2011.10.059.

Wahlgren, J., De L Karlson, T., Brisslert, M., Vaziri Sani, F., Telemo, E., Sunnerhagen, P., and Valadi, H. (2012). Plasma exosomes can deliver exogenous short interfering RNA to monocytes and lymphocytes. Nucleic Acids Res. *40*, e130. https://doi.org/10.1093/nar/gks463.

Wang, M.J., Yi, S., Han, J.Y., Park, S.Y., Jang, J.W., Chun, I.K., Kim, S.E., Lee, B.S., Kim, G.J., Yu, J.S., et al. (2017). Oligomeric forms of amyloid-β protein in plasma as a potential blood-based biomarker for Alzheimer's disease. Alzheimers Res. Ther. *9*, 98. https://doi.org/10.1186/s13195-017-0324-0.

STAR★METHODS

KEY RESOURCES TABLE

REAGENT or RESOURCE	SOURCE	IDENTIFIER
Antibodies		
mouse monoclonal anti-beta amyloid 1-42, clone 12F4 biotinylated mouse monoclonal anti-beta amyloid 1-42, clone 12F4	Biolegend Biolegend	Cat# 805501; RRID: AB_2564683 Cat# 805504; RRID: AB_2564688
goat anti-rabbit HRP	Invitrogen	Cat# 65-6120; RRID: AB_2533967
donkey IgG AF594	Life Technologies	Cat# A21209; RRID: AB_2535795
rabbit monoclonal anti-beta amyloid, clone D54D2	Cell Signaling Technology	Cat# 8243S; RRID: AB_2797642
rabbit monoclonal anti-alpha synuclein, clone MJFR1 rabbit monoclonal anti-alpha synuclein PE, clone MJFR1	abcam abcam	ab138501; RRID: AB_2537217 ab209306
Biological samples		
Human cerebrospinal fluid		
Human cerebrospinal fluid, Parkinson's disease donor	PrecisionMed	990201rev1
Human cerebrospinal fluid, Parkinson's disease donor	BIOIVT	HUMANCSF-0040179
Chemicals, peptides, and recombinant proteins		
lyophilized monomeric Aβ42 peptide	Anaspec	Cat# AS-72214
lyophilized monomeric HiLyte Fluor 488 Aβ42 peptide	Anaspec	Cat# AS-60479
Recombinant human alpha synuclein monomers	Proteos	RP-003
Critical commercial assays		
aldehyde sulfate beads (4 μm)	ThermoFisher Scientific	Cat# A37304, lot 1965879
streptavidin PE	eBioscience	Cat# 12-4317-87
assay buffer A	Anaspec	Cat# AS-72214
Miltenyi pan B cell isolation kit II	Miltenyi	Cat# 130-104-443
thick walled polycarbonate tubes	Beckman Coulter	Cat# 343775
bicinchoninic acid (BCA) protein assay kit	Pierce	Cat# 23227
4-15% tris-glycine gels	Bio-Rad	Cat# 4568086
amyloid beta 42 human ELISA kit	ThermoFisher Scientific	Cat# KHB 3441
imperial protein stain	ThermoFisher Scientific	Cat# 24615
ENrich SEC 650 column	Bio-Rad	Cat# 7801650
Protein LoBind 1.5 mL microcentrifuge tubes	Eppendorf	Cat# 022431081
Immun-Blot PVDF membrane	Bio-Rad	Cat# 1620177
SuperSignal West Pico PLUS ECL reagents	ThermoFisher Scientific	Cat# 34580
Experimental models: organisms/strains		
C57BL/6 mouse	The Jackson Laboratory	https://www.jax.org
Software and algorithms		
Flowjo	Becton-Dickinson	https://www.flowjo.com
Image J, version 1.51	National Institutes of Health	https://imagej.nih.gov/ij/download.html

(*Continued on next page*)

Continued

REAGENT or RESOURCE	SOURCE	IDENTIFIER
Prism, version 8.1.1	GraphPad	https://www.graphpad.com/scientific-software/prism/
Photoshop 2018	Adobe	https://www.adobe.com/products/photoshop.html
Image Lab	Bio-Rad	https://www.bio-rad.com/en-us/product/image-lab-software?ID=KRE6P5E8Z

RESOURCE AVAILABILITY

Lead contact

Further information and requests for resources and reagents should be directed to and will be fulfilled by the lead author, Thomas L. Rothstein (tom.rothstein@med.wmich.edu).

Materials availability

This study did not generate new unique reagents.

Data and code availability

- All data reported in this paper will be shared by the lead contact upon request.
- This paper does not report original code.
- Any additional information required to reanalyze the data reported in this paper is available from the lead contact upon request.

EXPERIMENTAL MODEL AND SUBJECT DATA

Mouse model

Female and male wild type 8 - 12 week old C57BL/6 mice (The Jackson Lab) were maintained under standard conditions in the vivarium at Western Michigan University Homer Stryker M.D. School of Medicine (WMED) and utilized experimentally in accordance to protocols approved by Institutional Animal Care and Use Committee at WMED.

Human cerebrospinal fluid

This study involved the use of human cerebrospinal fluid collected with consent from healthy donors in accordance to protocols approved by the Institutional Review Board at the Feinstein Institute for Medical Research. Parkinson's disease patient CSF from a 77 year old male and 60 year old male were purchased from PrecisionMed and Bio IVT, respectively.

METHOD DETAILS

Mouse splenic B cells

Whole spleens from C57BL/6 mice were first homogenized by gentle mechanical disruption with a syringe plunger and 70 μm mesh filter. B cells were subsequently isolated using the Miltenyi Pan B Cell Isolation Kit II (Miltenyi), in accordance to the manufacturer's instructions.

Conjugation of antibody to aldehyde sulfate beads

Aldehyde sulfate beads (4 μm) (ThermoFisher) were resuspended in phosphate buffered saline (PBS) at a concentration of 2 μL bead stock/50 μL PBS (unless otherwise indicated). Anti-beta amyloid 1-42 monoclonal antibody (clone 12F4 mAb; Biolegend) was prepared at 0.8 μg/50 μL PBS (unless otherwise indicated). The solutions were combined in a 1.5 mL microcentrifuge tube, mixed gently by pipet, and incubated for 40 min at room temperature. To quench unoccupied binding sites on the beads, 1000 μL PBS was added to the solution, followed by 110 μL of 1 M glycine. After a 15 min incubation at room temperature, 400 μL ice-cold blocking buffer (PBS/0.5% bovine serum albumin (BSA)/2 mM ethylenediaminetetraacetic acid (EDTA)) was added, and the solution was rotated for an additional 15 min. The sample was centrifuged at 4000 revolutions per minute (rpm) (Eppendorf tabletop centrifuge 5424R) for 3 min at 4°C and the supernatant was removed by pipet. These conditions were utilized for all experiments to pellet the beads. To wash the beads and remove unbound 12F4 mAb in solution, the bead pellet was gently resuspended in 400 μL ice-cold blocking buffer and centrifuged. The beads were washed two additional times. After the final wash, the pellet was resuspended in 400 μL ice-cold blocking buffer. The resultant solution contained enough antibody-coated beads for 20 sample tests (20 μL/test at 0.04 μg 12F4 mAb/0.1 μL bead stock).

Preparation of Aβ42 multimers

Lyophilized monomeric Aβ42 (Anaspec) was prepared in assay buffer A (Anaspec) in Protein LoBind 1.5 mL microcentrifuge tubes (Eppendorf), according to the manufacturer's instructions. Fluorescently labeled monomeric Aβ42 (HiLyte Fluor 488 Aβ42; Anaspec) was reconstituted in 1% NH_4OH and PBS as described by the manufacturer. To generate Aβ42 multimers, monomeric solutions (100 μL at 0.2125 μg/μl, unless otherwise indicated) were incubated at 1000 rpm/37 °C (ThermoMixer, Eppendorf) for the indicated period of time. The samples were then placed on ice for approximately 15 min and used for the assay, or frozen at −80°C for future use. All Aβ42 monomer or multimer solutions were kept on ice for the duration of test sample preparation. Solutions containing Aβ42 monomers or multimers were kept in LoBind tubes for all stages of the assay and during storage.

Binding of Aβ42 to 12F4 mAb-activated aldehyde sulfate beads

Aβ42 test samples were prepared in 20 μL assay buffer A (unless otherwise indicated). Antibody-coated beads (in 20 μL ice-cold blocking buffer, unless otherwise indicated) were combined with the test samples, gently mixed by pipet, and incubated for 60 min at room temperature, with mixing at 30 min to re-disperse the beads in solution. Ice-cold blocking buffer (400 μL) was then added to each tube, followed by centrifugation and one wash. After the final spin, all supernatant was removed by pipet, less approximately 25 μL to maintain bead hydration.

Detection of bead-captured Aβ42

Pelleted 12F4 mAb activated beads were resuspended in 50 μL biotinylated 12F4 mAb (Biolegend; prepared at 2.5 μg/mL in blocking buffer) and incubated for 60 min at room temperature, with mixing by pipet at 30 min. After addition of 400 μL ice-cold blocking buffer, the sample was centrifuged, washed, and centrifuged again, after which all supernatant was removed by pipet, less approximately 25 μL. The pellet was resuspended in 50 μL of streptavidin PE (eBioscience; prepared at 0.5 μg/mL in blocking buffer), mixed gently by pipet, and incubated for 20 min on ice, protected from light. Ice-cold blocking buffer (400 μL) was then added, and the sample was centrifuged, washed, centrifuged, and resuspended in 250 μL ice-cold blocking buffer for flow cytometry analysis.

Flow cytometry acquisition and analysis

All samples were acquired on a Fortessa Analyzer (Becton-Dickinson) at the low setting, yielding approximately 60–90 events/second for 0.1 μL bead stock/250 μL blocking buffer preparations. An FSC and SSC event threshold of 200 and voltage setting of 120 was utilized for all experiments. At least 4000 events of the gated bead population were acquired for each sample, and all analysis was conducted using Flowjo software (Becton-Dickinson). The gating scheme to identify the bead population for analysis, unless otherwise indicated, proceeded as: first gate on low FSC beads (FSC-A and SSC-A), second gate on single beads (FSC-A and FSC-W), third gate on single beads (SSC-A and SSC-W), and fourth gate on PE^+ beads (PE and SSC-A), defined against the negative control.

Microscopy imaging of aldehyde sulfate beads and B cell isolation

Aldehyde sulfate beads were prepared at a concentration of 1.0 x 10^6 beads/100 μL ice-cold blocking buffer, aliquoted to a standard 48 well plate, and imaged by brightfield microscopy using a Lionheart FX automated live cell imager (Biotek). To stain beads directly for fluorescent imaging, 4 μL beads were combined with 4 μg donkey anti-rat IgG AF594 (Life Technologies) in 50 μL PBS, followed by a 40 min incubation at room temperature. The sample was quenched with ice-cold blocking buffer, washed three times, and resuspended at a concentration of 1.0 x 10^6 beads/100 μL ice-cold blocking buffer for imaging. B cells were isolated from C57BL/6 whole spleen single cell suspensions using the Miltenyi Pan B Cell Isolation Kit II (Miltenyi) and prepared at 1.0 x 10^6 beads/100 μL ice-cold blocking buffer. Fluorescent beads and B cells were then mixed at a ratio of 50 μL:50 μL in a 48 well plate, incubated for 40 min, and imaged.

Isolation of Aβ42 multimers by centrifugation

Aβ42 monomers (0.25 μg/μl assay buffer A) were placed on ice, or incubated for 30 min or 60 min (2 x 100 μL/condition) at 1000 rpm/37°C to form multimers. The multimer samples were transferred to thick-wall polycarbonate tubes (Beckman Coulter) and subjected to centrifugation at 20,000 rpm (15,456 × g) for 30 min (Optima Max-TL Tabletop Ultracentrifuge (Beckman Coulter); TLA-100 fixed-angle rotor (Beckman Coulter)). Supernatant (100 μL) was removed carefully from the 30 min sample so as to not disturb the pellet, and placed on ice. For the 60 min sample, supernatant was removed by pipet and the pellet was resuspended in 200μL assay buffer A. Following a second spin (20,000 rpm × 30 min), all supernatant was removed carefully, and the pellet was resuspended in 40 μL assay buffer A. The protein concentration of each sample was determined by the bicinchoninic acid (BCA) method according to the manufacturer's directions (Pierce).

Native polyacrylamide gel electrophoresis (PAGE) and immunoblot

Samples were prepared 1:2 in 2× native sample buffer (62.5 mM Tris-HCl pH 6.8, 40% glycerol, 0.01% bromophenol blue) and resolved on 4-15% tris-glycine gradient gels (Bio-Rad). Sodium dodecyl sulfate (SDS) was excluded from the running buffer. The gels were stained with coomassie blue-based Imperial protein stain (Thermo Scientific) for 60 min at room temperature with gentle agitation, followed by several destain cycles in ultrapure water. Gel imaging and acquisition was completed on the chemidoc imaging system (Bio-Rad). For immunoblot detection of Aβ42, gels were equilibrated in Bjerrum transfer buffer (48 mM Tris, 39 mM glycine,

0.04% SDS in ultrapure water) for five minutes, and PVDF membranes (0.2 μm; Bio-Rad) were first activated in 100% methanol for two minutes and then equilibrated by a five minute incubation in transfer buffer. Transfer occurred at 100 V constant for 60 min on ice. The membrane was incubated in wash buffer (TBS/0.1% Tween-20) for five minutes after transfer, prior to a 60 min block in blocking buffer (wash buffer + 5% milk (w/v)). Incubation with monoclonal anti-Aβ42 (CST) in blocking buffer (1:1000) occurred overnight at 4°C. The membrane was then washed (20 min, three buffer changes) and incubated with goat anti-rabbit HRP (Invitrogen; 1:5000 in blocking buffer) for 40 min at room temperature. The membrane was subsequently washed for 30 min (five buffer changes) and then developed by enhanced chemiluminescence.

Spectrophotometry (turbidity) measurements

Samples of either Aβ42 or aldehyde sulfate beads (4 μm) were prepared in 100 μL buffer at the indicated amounts in 96 well microtiter plates. The plates were then subjected to absorbance measurements at 395 nm (A395).

Purification of Aβ42 oligomers and protofibrils by size exclusion chromatography

To form Aβ42 oligomers and protofibrils, 15 μM Aβ42 monomers were vortexed for 30 seconds and then incubated at 4°C for two weeks as previously described (Ryan et al., 2010). Samples were centrifuged at 14,000 × g for 10 min at 4°C to eliminate insoluble mature fibrils. Oligomers and protofibrils were purified by size exclusion chromatography as previously described with a minor modification (Esparza et al., 2016). Briefly, 0.25 mL of sample was injected onto an Enrich SEC 650 column (Bio-Rad) attached to an NGC Quest Chromatography system (Bio-Rad), and eluted with PBS containing filtered 0.05% BSA at a flow rate of 0.5 mL/min. A total of 19 1 mL elution fractions were collected and resolved by PAGE. Fractions 8 and 9 were pooled as protofibrils whereas fractions 11 and 12 were pooled as oligomers. The concentration of Aβ42 oligomers and protofibrils were determined by ELISA (Thermo Fisher Scientific).

Alpha synuclein aggregate formation and bead assay detection in human cerebrospinal fluid

Monomeric alpha synuclein (αS) (10 mg/mL in 10 mM Tris, 50 mM NaCl, pH 7.6; Proteos) was diluted 1:2 in 2X PBS, aliquoted in Lobind tubes, and either frozen (−80°C) or induced to aggregate according to the manufacturer's instructions (37°C/1000 rpm; also see Polinski et al., 2018). Prior to analysis by PAGE or the bead assay, both sample preparations were subjected to centrifugation to more thoroughly isolate the αS species of interest. Monomeric αS was transferred to thick-wall polycarbonate tubes and centrifuged in a TLA-100 fixed-angle rotor at 51,000 rpm (100,500 × g) for 40 min (4°C). The resultant supernatant was collected and either used immediately or frozen at −80°C. Aggregated αS was centrifuged at 10,000 × g for 30 min (4°C), and following removal of the supernatant, the pellet was washed in 200 μL PBS and centrifuged again at 10,000 × g for 30 min (4°C). The resultant pellet, designated as aggregated αS, was resuspended in 60 μL PBS and used immediately or frozen (−80°C). Protein concentration of both monomeric and aggregated samples was determined by BCA method, and titrated samples were then resolved by native PAGE as described above for Aβ42. Bead assay analysis of αS monomers and aggregates followed the protocol established for Aβ42, only here using anti-αS MJFR1 (abcam) and MJFR1-PE (abcam) as the capture and detection monoclonal antibodies, respectively. Human cerebrospinal fluid (CSF), from four normal individuals and stored in liquid nitrogen or two Parkinson's disease patients, was thawed on ice and centrifuged at 2000 × g for 20 min prior to use, with the supernatant utilized as the CSF stock. For experiments requiring diluted CSF, the CSF stock was prepared in buffer at the indicated concentration.

QUANTIFICATION AND STATISTICAL ANALYSIS

Prism software (version 8.1.1; GraphPad) was used to generate graphs and for statistical analyses. One-way ANOVA was performed for comparison of three or more groups to determine an overall difference, followed by a two-tailed t test between groups. Values of $p < 0.05$ were considered significantly different. Coomassie stained gels were imaged on the chemidoc imaging system (Bio-Rad). ImageLab software (Bio-Rad) or photoshop (Adobe) was used to process and prepare images. All adjustments or transformations during image preparation were equivalently applied to the whole image. Microscopy images acquired using the Lionheart FX automated live cell imager (Biotek) were processed using image J software (National Institutes of Health). All adjustments or transformations during image preparation were equivalently applied to the whole image. Final figure layouts were completed using photoshop software (version 2018; Adobe).